



DNASE1L3 inhibits hepatocellular carcinoma by delaying cell cycle progression through CDK2

Jiaqi Sun¹ · Xiyang Wang¹ · Qingsong Shen¹ · Min Wang¹ · Shuxian Chen¹ · Xuechun Zhang¹ · Yongping Huang¹ · Zhonglin Zhang² · Wenhua Li¹ · Yufeng Yuan² · Zan Huang¹

Accepted: 17 August 2022 / Published online: 3 November 2022
© Springer Nature Switzerland AG 2022

Abstract

Purpose Dysregulated cell cycle targeting is a well-established therapeutic strategy against hepatocellular carcinoma (HCC). Dissecting the underlying mechanism may improve the efficacy of HCC therapy.

Methods HCC data from TCGA and new clinical samples were used for DNASE1L3 expression analysis and for assessing its correlation with HCC development. The in vitro function of DNASE1L3 in HCC cell proliferation, colony formation, migration and invasion was assessed using RTCA, CCK-8 and transwell assays and the in vivo function in subcutaneous tumor formation in a xenograft nude mouse model. The role of DNASE1L3 in HCC tumorigenesis was further verified in AKT/NRASV12-induced and DEN/CCl₄-induced primary liver cancers in wildtype and *Dnase1l3*^{-/-} mice. Finally, RNA-Seq analysis followed by biochemical methods including cell cycle, immunofluorescence, co-immunoprecipitation and Western blotting assays were employed to reveal the underlying mechanism.

Results We found that DNASE1L3 was significantly downregulated and served as a favorable prognostic factor in HCC. DNASE1L3 dramatically attenuated HCC cell proliferation, colony formation, migration and invasion in vitro and reduced subcutaneous tumor formation in nude mice in vivo. Furthermore, DNASE1L3 overexpression dampened AKT/NRASV12-induced mouse liver cancer in wildtype mice and DNASE1L3 deficiency worsened DEN/CCl₄-induced liver cancer in *Dnase1l3*^{-/-} mice. Systemic analysis revealed that DNASE1L3 impaired HCC cell cycle progression by interacting with CDK2 and inhibiting CDK2-stimulated E2F1 activity. C-terminal deletion (DNASE1L3^{ΔCT}) diminished the interaction with CDK2 and abrogated the inhibitory function against HCC.

Conclusion Our study unveils DNASE1L3 as a novel HCC cell cycle regulator and tumor suppressor. DNASE1L3 impairs HCC tumorigenesis by delaying cell cycle progression possibly through disrupting the positive E2F1-CDK2 regulatory loop. DNASE1L3 may serve as a target for the development of novel therapeutic strategies against HCC.

Keywords Hepatocellular carcinoma · DNASE1L3 · Cell cycle · CDK2

1 Introduction

The diagnosis of hepatocellular carcinoma (HCC) at advanced stages is relatively frequent and targeted therapies for unresectable HCC at these stages have limited efficacy with adverse events and frequent resistance, both

of which result in a poor prognosis and urge for development of novel therapies [1, 2]. Dissecting molecular mechanisms and identifying novel pathogenic gene alterations are imperative for the development of therapeutic targets with a high efficacy [3, 4]. Uncontrolled proliferation due to cell cycle dysregulation is one of the hallmarks of cancer and a well-established target for cancer therapy. The cell cycle is a tightly organized biological process and coordinately regulated by various cyclin/cyclin dependent kinase (CDK) complexes [5]. However, overexpression of cyclins including Cyclin D [6] and Cyclin E [7] and overactive cyclin-dependent kinases [6, 7] are frequently observed in many types of cancer. In HCC, a subtype of “proliferative class” is characterized by HBV infection, p53 mutations, and

✉ Zan Huang
z-huang@whu.edu.cn

¹ College of Life Sciences, Hubei Key Laboratory of Cell Homeostasis, Wuhan University, Wuhan, China

² Department of Hepatobiliary and Pancreatic Surgery, Zhongnan Hospital of Wuhan University, Wuhan, China

enrichment of cell cycle signatures including *CDKN2A* loss, *CCND1* amplification, E2F1 activation and *CCNE1* overexpression [8–10]. Unfortunately, this knowledge has barely been translated into clinical therapies against HCC.

DNASE1L3 (deoxyribonuclease I like 3) is an endonuclease and belongs to the deoxyribonuclease I (DNase I) family [11]. DNASE1L3 can digest DNA in serum [12] and in liposomes [13], genomic DNA with native polynucleosomes, and chromatin in apoptotic cell-derived microparticles as well as in necrotic cells [14]. *DNASE1L3* mutations are tightly associated with systemic lupus erythematosus (SLE) and scleroderma (SSc) [14, 15]. DNASE1L3 inhibits NET vascular occlusion by degrading DNA fibers [16]. Recent studies have shown that DNASE1L3 may also serve as a biomarker in breast, liver, lung, colon and stomach cancer [17, 18] and as a favorable prognostic factor for HCC [19]. DNASE1L3 has been shown to play roles in immune escape and senescence-induced angiogenesis in HCC cells [17, 20]. However, the *in vivo* function and the underlying mechanism of DNASE1L3 in HCC tumorigenesis have not been systemically investigated and verified.

Here, we found DNASE1L3 down regulation is tightly associated with HCC development and that DNASE1L3 functions as a cell cycle regulator and tumor suppressor both *in vitro* and *in vivo*. More importantly, we found that DNASE1L3 impaired HCC tumorigenesis by delaying cell cycle progression, possibly through interacting with CDK2 and disrupting a positive E2F1-CDK2 regulatory loop. DNASE1L3 may serve as a target for the development of novel therapeutic strategies directed against HCC.

2 Materials and methods

2.1 Cell culture and animal models

The human cell lines L02, HCCLM9, Huh7, MHCC97H, Hep3B and HEK293T were previously maintained in our laboratory and maintained in the complete Dulbecco's modified Eagle medium (DMEM, Gibco) with 10% fetal bovine serum (FBS, Cegrogen) and 1% penicillin and streptomycin (Gibco). DNASE1L3 knockout mice (*Dnase1l3*^{-/-}, C57BL/6 background) were generated using the CRISPR/Cas9 technique. Briefly, the sequence targeting the mouse *Dnase1l3* gene was predicted by the online CRISPR design tool (<http://crispr.mit.edu/>) as follows: GTCCTTTGGAGCGAGCAAGAAGG. Two complementary single-stranded oligos were synthesized, annealed and ligated into a pUC57-sgRNA vector to construct a sgRNA expression vector. The DNA fragment containing the T7 promoter and the guide sequence was amplified by PCR for *in vitro* transcription. The transcribed Cas9 mRNA and

sgRNA were injected into single-cell fertilized eggs of C57BL/6 mice using a FemtoJet 5247 microinjection system, which were subsequently transplanted into surrogate female mice in the fallopian tubes. Two weeks after delivery, genomic DNA from founder mice (F0) was extracted for PCR and sequencing. Mice with frameshift mutations were crossed with wild-type mice to generate heterozygous mice (*Dnase1l3*^{+/-}, F1), which were further used for crossing to generate homozygous *Dnase1l3*^{-/-} mice. The following primer set was used for PCR amplification to produce a 409-bp product for sequencing: *Dnase1l3*-F: 5'-AAGTCAGTGAGCCAGGCACT-3', *Dnase1l3*-R: 5'-AAGCACAGATCCACCCAGTC-3'. WT and *Dnase1l3*^{-/-} male mice (8–10 weeks old) were used for further experiments. Female C57BL/6 nude mice (4–6 weeks old) were used for xenografting. All animal experiments were approved by the Animal Care and Use Committee of the College of Life Sciences of Wuhan University. Care was provided following the criteria outlined in the Guide for the Care and Use of Laboratory Animals prepared by the National Academy of Sciences and published by the National Institutes of Health.

2.2 Analysis of TCGA data

HCC data from The Cancer Genome Atlas (TCGA) database were downloaded for analysis of DNASE1L3 expression and its correlation to the stage and survival rate of HCC patients.

2.3 Clinical sample acquisition

HCC tumor tissues and the paired adjacent non-tumor tissues were collected from Zhongnan Hospital of Wuhan University, Wuhan, China. Procedures involving human samples were approved by the Zhongnan Hospital of Wuhan University Review Board and were consistent with the principles outlined in the *Declaration of Helsinki*. Written informed consent was obtained from each patient. Samples were used for quantitative RT-PCR and Western blotting to detect the mRNA and protein levels of DNASE1L3, respectively, in tumor tissues and paired adjacent non-tumor tissues.

2.4 Cell proliferation assays

RTCA (Real-Time Cell Analysis) as the xCELLigence Cell Function Analyzer (DP System) was used to measure cell proliferation. Briefly, adherent cells were resuspended in complete DMEM medium (Gibco) at a density of 4.0×10^4 /mL. Then, an E-Plate View 16 was filled with 50 μ L complete DMEM medium to check the baseline. Next, 100 μ L cell suspension was added to the plate. Cell proliferation was monitored over time following the

manufacturer's instructions. CCK8 (Cell Counting Kit-8) was also used for cell proliferation analysis. Adherent cells were resuspended in complete DMEM medium at a density of 4.0×10^4 /mL. Then, 100 μ L cell suspension was added to 96-well plates and 10 μ L CCK8 test solution was added. The solution was equilibrated for 2 h at 37°C. Finally, the absorbance was measured at 450 nm.

2.5 Cell migration assays

RTCA was used to measure cell migration. Briefly, 165 μ L complete DMEM was added to the bottom of a CIM-Plate. The upper chamber was filled with 30 μ L DMEM without serum and equilibrated for 1 h at 37°C after which the baseline was detected. Cells were resuspended in DMEM medium without serum at a density of $5\text{--}10 \times 10^5$ /mL after which 100 μ L of the cell suspension was added to the upper chamber. Cell migration was monitored over time following the manufacturer's instructions. A transwell assay was also used for cell migration assessment. Adherent cells were resuspended in DMEM without serum at a density of 1.2×10^5 /mL after which 500 μ L of the cell suspension was added to the transwell chamber. 600 μ L complete DMEM was added to the bottom of the plate. After 24 h, the transwell chamber was taken out, washed with PBS, and stained with 0.05% crystal violet for 45 min. The upper layer of cells was wiped off and randomly selected microscopic fields were used for counting migrated cells by Image J software.

2.6 Cell invasion assay

A transwell assay was used to measure cell invasion. To this end, the transwell chambers were coated with 100 μ L 200 μ g/mL Matrigel and equilibrated for 3 h at 37°C. Adherent cells were resuspended in DMEM without serum at a density of 1.2×10^5 /mL after which 500 μ L of the cell suspension was added to the transwell chamber. 600 μ L complete DMEM was added to the bottom of the plate. After 48 h, the transwell chambers were taken out and washed with PBS followed by staining with 0.05% crystal violet for 45 min. After wiping off the upper layer of cells, the invasive cells were observed under a microscope and cell numbers in randomly selected fields were counted by Image J software.

2.7 Colony formation assay

Adherent cells were resuspended in complete DMEM at a density of $2\text{--}4 \times 10^4$ /mL. Then, 100 μ L of the cell suspension was added to a 6-well plate. After 7–10 days, the plate was washed with PBS and fixed with 4% paraformaldehyde

for 30 min at room temperature. Next, the plate was stained with 0.1% crystal violet for 20 min and scanned by a scanner. Colony numbers were counted by Image J software.

2.8 Co-immunoprecipitation and Western blotting

Co-immunoprecipitation and Western blotting were performed as previously described [21, 22]. In brief, cells (3×10^6) were collected and lysed in 200 μ L lysis buffer. Cell lysates were incubated with 15 μ L protein A/G beads and 1 μ L indicated primary antibody overnight. After extensive washing, the immunocomplexes were eluted in loading buffer. For western blotting, total cell lysates were prepared in RIPA buffer and the protein concentration was determined using a BCA Protein Assay Kit (Beyotime). Next, protein separation on 10% polyacrylamide gels and electronic transfer onto PVDF membranes (Millipore) were performed. After blocking, the membranes were incubated with primary antibodies (1:1000) at 4°C overnight followed by washing and incubation with secondary antibodies labeled with horseradish peroxidase (HRP) for 1 h. After washing, an Enhanced ECL Chemiluminescence Detection Kit (Vazyme, Cat#E412) was used and the signals were detected by a ChemiDoc MP Imaging System (Tanon-5200, Tanon). The antibodies used for immunoprecipitation (IP) and Western blotting were: anti-DNASE1L3 (GeneTex, Cat#GTX114363), anti-CDK2 (Abcam, Cat#ab32147), anti-CyclinD1 (Abclonal, Cat#A19038), anti-CDC25C (Abclonal, Cat#A12234), anti- β -actin (ProteinTech, Cat#66,009), anti-DYKDDDDK (MBL, Cat#MAB8529), anti-HA (ProteinTech, Cat#51,064), anti-LaminA/C (CST, Cat#4777), HRP AffiniPure Goat Anti-Mouse IgG (Fdbio, Cat#FD0142) and HRP AffiniPure Goat Anti-Rabbit IgG (H + L) (Fdbio, Cat#FD0128).

2.9 Quantitative RT-PCR

Total RNA was extracted with TRIzol reagent (Vazyme, Cat#R401-01) and used for reverse-transcription employing a MonScript™ RTIII Super Mix (Monad, Cat#MR05201). Quantitative PCR was performed on a Fast Real-time PCR System (Monad, China). The following cycle was used for PCR: hot-start at 95°C for 60 s followed by 95°C for 30 s, 60°C for 30 s, for 40 cycles. The primer sets used are provided in the Supplemental data and information.

2.10 Subcutaneous tumor formation assay

Female BALB/C nude mice (four weeks old, purchased from HFK) were used for subcutaneous tumor formation. Control and DNASE1L3 overexpressing HCCLM9 cells were resuspended at a density of about 5×10^6 cells in 100 μ L

PBS. Matrigel was thawed at 4 °C and mixed with the cells in a ratio of 1:1. Next, 200 µL of the mixture was injected into the axilla of the right forelimb of a nude mouse. The mice were examined every week for tumor growth and sacrificed when the tumor volume reached 1000 mm³ (tumor volume (mm³) = 0.5 × length (mm) × width (mm)²).

2.11 Mouse liver cancer models

Hydrodynamic injection of transposon-based vectors overexpressing constitutively active AKT (myr-AKT) and NRASV12 and a vector overexpressing transposase through tail veins in mice was used to cause integration of the myr-AKT and NRASV12 expression cassettes into the genomes of hepatocytes. Stable overexpression of myr-AKT and NRASV12 is known to induce primary liver cancer [23, 24]. Male C57BL/6 mice (HFK) around 8 weeks old were used. pT3-myr-AKT-HA (Addgene #31,789), pT/Caggs-NRASV12 (Addgene #20,205) and pCMV (CAT) T7-SB100 (Addgene #34,879) in combination with pT3-DNASE1L3 or pT3-control vectors were injected into the tail veins at high pressure within 5–7 s. The mice were examined every week and sacrificed when 16 weeks old.

Mouse liver cancer was also induced by diethylnitrosamine (DEN) and carbon tetrachloride (CCl₄) treatment in wild type (WT, C57BL/6 background) and *Dnase1l3* knockout (*Dnase1l3*^{-/-}) male mice. The mice were intraperitoneally injected with DEN (N0258, Sigma, 25 mg/kg) when 2 weeks old. CCl₄ (0.5 mL/kg) was administered every other day through gavage from the age of 8 weeks to 21 weeks. The mice were examined every week and sacrificed when 22 weeks old.

2.12 Alanine transaminase (ALT) and aspartate aminotransferase (AST) detection

ALT and AST in serum were detected using specific kits (NJJC, C009-2-1 and NJJC, C010-2-1) following the manufacturer's instructions.

2.13 Hematoxylin-eosin (H&E) and picric sirius red (PSR) staining

Fresh liver tissues were placed in 10% neutral formalin and fixed overnight. The fixed tissues were processed by dehydration, transparency, wax immersion and embedding. Next, tissues were sectioned into 5-µm slides with a paraffin microtome. Hematoxylin-eosin staining solution was used for H&E staining and picric sirius red staining solution was used for PSR staining.

2.14 Oil red O staining

Fresh liver tissues were embedded in OCT matrix and stored at -80°C before use. Tissues were sequentially frozen-sectioned, air-dried, fixed with 4% formalin, decolorized in propylene glycol, stained in oil red solution, differentiated, and re-stained with hematoxylin. Glycerin and cover glasses were mounted onto the slides before evaluation under a microscope.

2.15 RNA-Seq (RNA sequencing) analysis

Total RNA was extracted from DEN/CCl₄-induced WT and *Dnase1l3*^{-/-} mouse liver tumors after which the RNA quality was evaluated by gel separation. Qualified RNA was diluted to 300 ng/µL for library preparation and sequencing following the manufacturer's instructions. After sequencing, the soap (v2.2.1) software developed by BGI was used to control the quality of the offline reads. Then hisat2 (v2.1.0) software was used to map the reads to the reference mouse genome (version mm10). Samtools (v1.4) was used to convert and sort the mapping results and the fpkm value calculation by string-tie (v1.3.3b) software was used for gene expression quantification. Differences in gene expression were calculated using R package *deseq2* (v1.22.2) and gene volcano scatterplots were generated using the fold change (x-axis, log₂) and *p* value (y-axis) of each gene. Genes with an adjusted *p* value < 0.05 and variance multiple > 2 were considered as being differentially expressed.

2.16 Cell cycle assay

HCCLM9 cells (5 × 10⁶) were seeded in a 6-well plate and synchronized at the G1 phase by serum starvation for 24 h or synchronized at the G2/M phase by nocodazole treatment (35 ng/mL) (M1404, Sigma) for 20 h. The synchronized cells were released by changing the medium with fresh complete medium without any drug for 2 h. Next, the cells were harvested, resuspended in 400 µl PBS and fixed in 500 µL 70% pre-cooled ethanol at 4°C overnight. The cells were stained with PI (60 µg/mL) (P4107, Sigma) for 1 h for flow cytometric cell cycle analysis using Flowjo.

2.17 Dual luciferase activity assay

HEK293T cells were co-transfected with different combinations of E2F1-driven firefly luciferase reporter vector, DNASE1L3 overexpression vector, CDK2 overexpression vector, control vector and internal renilla luciferase overexpression vector. Cells were washed with PBS three times and lysed in lysis buffer for 30 min at room temperature. A luciferase kit (Promega E1960) and Promega Max

20/20 was used to measure the firefly and renilla luciferases activities.

2.18 Preparation of cytoplasmic and nuclear extracts

HCCLM9 cells (3×10^7) were incubated in 1 ml hypotonic buffer (10 mM Tris (pH 7.4), 1.5 mM $MgCl_2$, 10 mM KCl, 0.5 mM DTT, 0.5 mg/ml Pefabloc, 0.1% NP40) on ice for 20 min. After centrifugation at 5500 g at 4°C for 10 s, the upper layer was transferred to a new tube as cytoplasmic extract. The pellet with nuclei was washed with hypotonic buffer 3 times and lysed in 500 μ L lysis buffer (10 mM Tris-HCl (pH 7.4), 150 mM NaCl, 1% NP40, 0.5% sodium deoxycholate, 1 mM EDTA, 1 mM DTT). After ultrasonication (3 s, 3 s, 10 times, 4°C) the lysate was centrifuged at 12,000 g for 10 min at 4°C. The upper layer was transferred to a new tube as nuclear extract.

2.19 Immunofluorescence assay

HCCLM9 cells (1×10^5) were seeded on slides in a 24-well plate and cultured for 24 h. Next, the cells were fixed in 4% formaldehyde for 15 min and permeabilized with 0.1% Triton-X 100 for 15 min at room temperature. Then, the cells were washed with PBS three times and blocked with 5% BSA/PBS for 30 min followed by incubation with primary antibody (1:500, in 5% BSA/PBS) for 1 h at room temperature. After washing with PBS three times, the cells were incubated with secondary antibody (1:200, in 5% BSA/PBS) for 1 h at room temperature in the dark. The slides were mounted with an anti-bleaching mounting agent after washing.

2.20 Statistical analysis

All data were analyzed using Graphpad software and expressed as the mean \pm SEM. Student's *t* test was employed to analyze differences between two groups. Shapiro-Wilk normality was used to analyze the normality of each group. Student *t* test was used for normally distributed data and Mann-Whitney test was used for non-normally distributed data. One-way ANOVA was applied for multiple comparisons under one factor. Shapiro-Wilk was used to analyze the normality of each group. When the data were normally distributed, Bonferroni's multiple comparisons test was used. When the data were non-normally distributed, the Dunnett's T3 multiple comparison test was used. Two-way ANOVA and Bonferroni's tests were applied for multiple comparisons under two factors. A *p* value < 0.05 was defined as significant difference between two groups. The statistical

methods and comparison significances are shown in the figure legends.

3 Results

3.1 DNASE1L3 downregulation is tightly associated with HCC development

HCC data from TCGA were used to explore a potential correlation between DNASE1L3 expression and HCC development. We found that *DNASE1L3* was significantly downregulated in HCC tumors compared to the normal tissues (Fig. 1A). The *DNASE1L3* expression level was negatively correlated to cancer stage (Fig. 1B) and positively correlated to overall survival (Fig. 1C) and disease-free survival (Fig. 1D). Consistently, we found that the DNASE1L3 protein level was downregulated in a HCC tissue array (Fig. 1E). Furthermore, we verified downregulation of *DNASE1L3* mRNA expression in freshly collected HCC tumors (T) compared to the paired adjacent non-tumor tissues (NT) (Fig. 1F). We found that 9 out of 13 HCC tumors showed downregulation of DNASE1L3 protein expression (Fig. 1G). In addition, we found that both mRNA and protein expression levels of DNASE1L3 in HCC cell lines were relatively low in comparison to that in the non-transformed liver cell line L02 (Fig. 1H and 1I). Taken together, these observations indicate that DNASE1L3 is downregulated and serves as a favorable prognostic factor in HCC.

3.2 DNASE1L3 suppresses HCC cell proliferation, colony formation, migration and invasion in vitro

To test the function of DNASE1L3 in HCC, we knocked down DNASE1L3 using a CRISPR/dCas9-KRAB technique in HCCLM9 cells (Fig. 2A-B). We found that DNASE1L3 knockdown promoted HCCLM9 cell proliferation, colony formation, migration and invasion in HCCLM9 cells (Fig. 2C-F). In contrast, we found that DNASE1L3 overexpression inhibited cell proliferation, migration and invasion in HCCLM9 and Huh7 cells (Fig. 2G-L and Fig. S1A-C). DNASE1L3 possesses DNA endonuclease activity and deletion of its C-terminal sequence (DNASE1L3^{ACT}) leads to deficient enzyme activity [14]. We found that DNASE1L3^{ACT} lost the ability to suppress HCCLM9 cell proliferation and colony formation (Fig. 2M-O), migration (Fig. 2P and Fig. S1D) and invasion (Fig. 2Q). These results suggest that DNASE1L3 plays a suppressive role in HCC development and that its C-terminal deletion impairs this function.

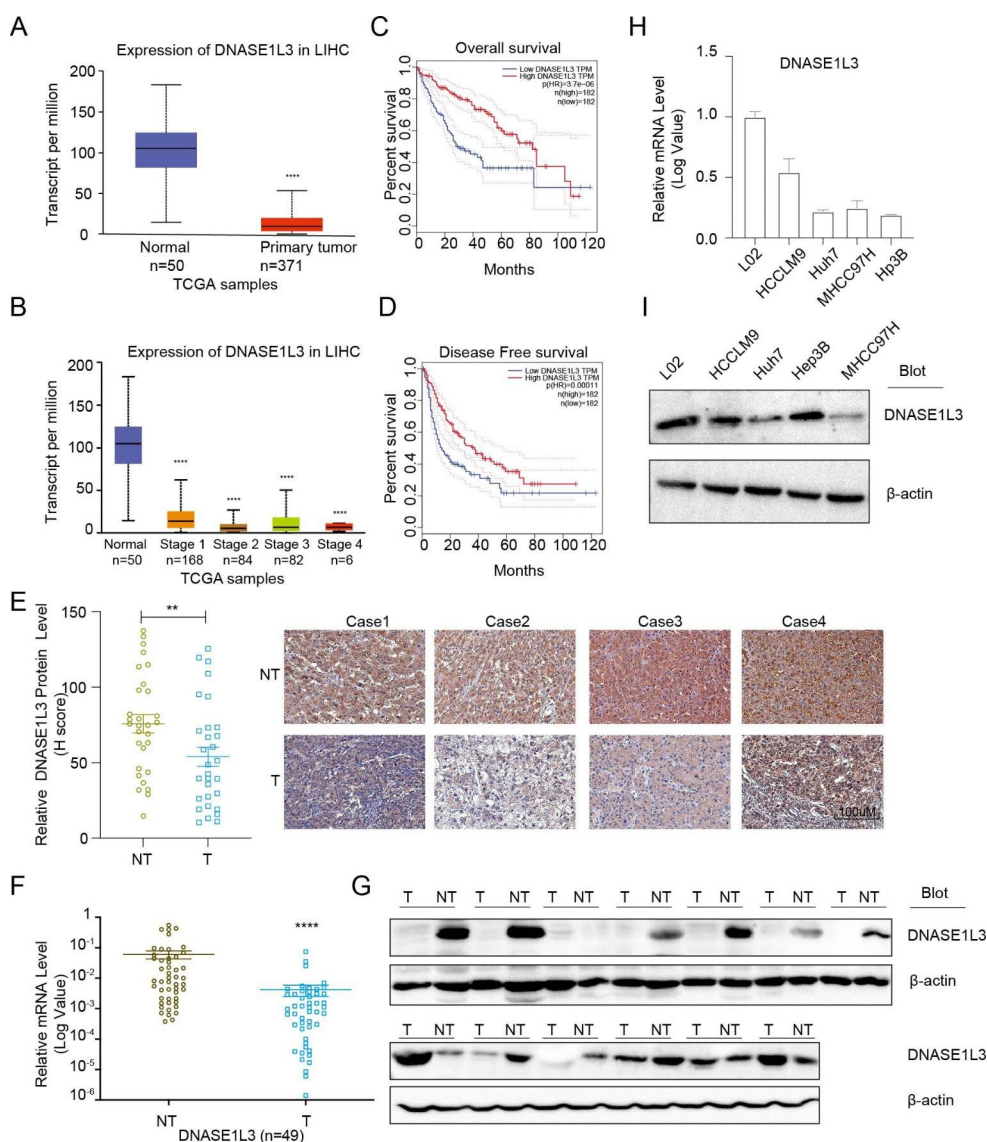


Fig. 1 DNASE1L3 downregulation is associated with HCC (A) Analysis of TCGA data showed downregulation of *DNASE1L3* in HCC tumors compared to normal tissues (tumor $n=371$; normal $n=50$). (B) Negative correlation of *DNASE1L3* expression level to HCC stage in TCGA data (Normal $n=50$, Stage 1 $n=168$, Stage 2 $n=84$, Stage 3 $n=82$, Stage 4 $n=6$). (C) Positive correlation of *DNASE1L3* expression and overall survival in TCGA data (High expression $n=182$, Low/media expression $n=182$). (D) Positive correlation of *DNASE1L3* expression and disease-free survival in TCGA data (High expression $n=182$, Low/media expression $n=182$). (E) Statistical analysis (left panel) and representative images (right panel) of *DNASE1L3* protein expression level measured by IHC in HCC tissue array (T: tumor; NT: the paired adjacent non-tumor tissues, $n=30$). (F-G) Downregulation of *DNASE1L3* mRNA and protein expression levels in HCC tumors.

3.3 DNASE1L3 inhibits HCC progression and tumorigenesis

To verify the *in vivo* function of *DNASE1L3* in HCC, we carried out xenograft experiments in nude mice. We found

Quantitative RT-PCR analysis of *DNASE1L3* mRNA expression level in HCC tumors and the paired adjacent non-tumor tissues (T: tumor; NT: the paired adjacent non-tumor tissues, $n=49$) (F). Representative immunoblotting analysis of *DNASE1L3* protein expression level in HCC tissues and the paired adjacent non-tumor tissues (T: tumor; NT: the paired adjacent non-tumor tissues) ($n=13$) (G). (H-I) Downregulation of *DNASE1L3* mRNA and protein expression levels in different HCC cells. Quantitative RT-PCR analysis of *DNASE1L3* expression levels (H) and immunoblotting analysis of *DNASE1L3* protein expression level (I) in different HCC cells. All data were presented as the mean \pm SEM. Data in (A) (E) (F) were analyzed by Students' *t* test. Data (B)(C)(D) were analyzed by one-way ANOVA. * $p<0.05$, ** $p<0.01$, *** $p<0.001$, **** $p<0.0001$

that *DNASE1L3* overexpression significantly reduced the size of subcutaneous tumors over time (Fig. 3A-B). In contrast, we found that *DNASE1L3*^{ΔCT} lost this ability comparable to its control (Fig. 3A-B). In addition, we tested the function of *DNASE1L3* in AKT/NRASV12-induced mouse

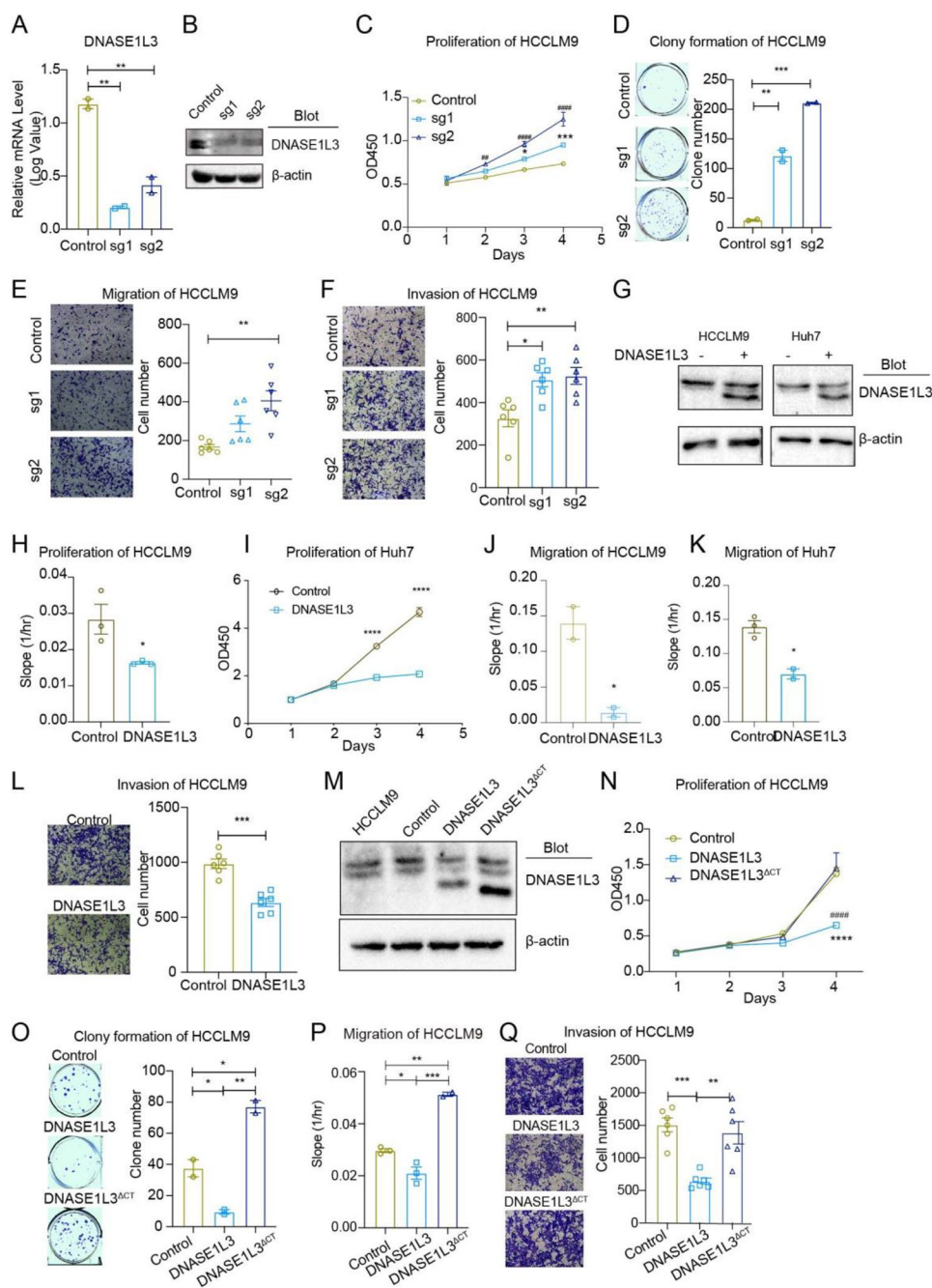


Fig. 2 DNASE1L3 suppresses HCC cell proliferation, migration, and invasion in vitro (**A–B**) The efficiency of DNASE1L3 knockdown in HCCLM9 cells was confirmed by quantitative RT-PCR (**A**) and immunoblotting analysis with antibodies as indicated (**B**). Two different guide sequences (sg1, sg2) were used. (**C–F**) DNASE1L3 deficiency promotes cell proliferation, colony formation, migration and invasion. Cell proliferation ($n=3$ per group) (**C**), colony formation ($n=2$ per group) (**D**), cell migration ($n=6$ per group) (**E**), and cell invasion ($n=6$ per group) (**F**) of HCCLM9 cells with DNASE1L3 knockdown were detected. The representative images (left panel) and statistical results (right panel) (**D–F**) were presented. (**G**) Immunoblotting analysis of DNASE1L3 overexpression in HCCLM9 and Huh7 cells with indicated antibodies. (**H–L**) DNASE1L3 overexpression inhibits cell proliferation, cell migration, and cell invasion of HCC cells. Proliferation of HCCLM9 cells (**H**) ($n=3$ per group) and Huh7 cells (**I**) ($n=3$ per group), migration of HCCLM9 cells (**J**) ($n=2$ per group) and Huh7 cells (**K**) ($n=3$ per group), and cell invasion of HCCLM9 cells (**L**) ($n=6$ per group) with DNASE1L3 overexpression were assayed. The

representative images (left panel) and statistical results of invasion (right panel) were shown (**L**). (**M**) Immunoblotting analysis of the overexpression WT and mutant DNASE1L3 Δ CT in HCCLM9 cells. (**N–Q**) C-terminal deletion impairs the inhibitory function of DNASE1L3 on HCC. Proliferation (* represents significant difference between Control and DNASE1L3 group, # represents significant difference between DNASE1L3 and DNASE1L3 Δ CT group, $n=3$ per group) (**N**), colony formation (right panel) ($n=2$ per group) (**O**), cell migration ($n=3$ per group) (**P**), and cell invasion ($n=6$ per group) (**Q**) of HCCLM9 cells overexpressing WT DNASE1L3 or mutant DNASE1L3 Δ CT were measured. The representative images (left panel) and statistical results (right panel) were shown (**O, P, Q**). The data except (**B**)(**G**)(**M**) were presented as the mean \pm SEM. Data in (**H**)(**J**)(**K**) and the right panel in (**L**) were analyzed by Student's *t* test. Data in (**A**)(**P**) and the right panel of (**D**)(**E**)(**F**)(**O**)(**Q**) were analyzed by one-way ANOVA. Data in (**C**)(**I**)(**N**) were analyzed by two-way ANOVA. * $p < 0.05$, ** $p < 0.01$, *** $p < 0.001$, **** $p < 0.0001$

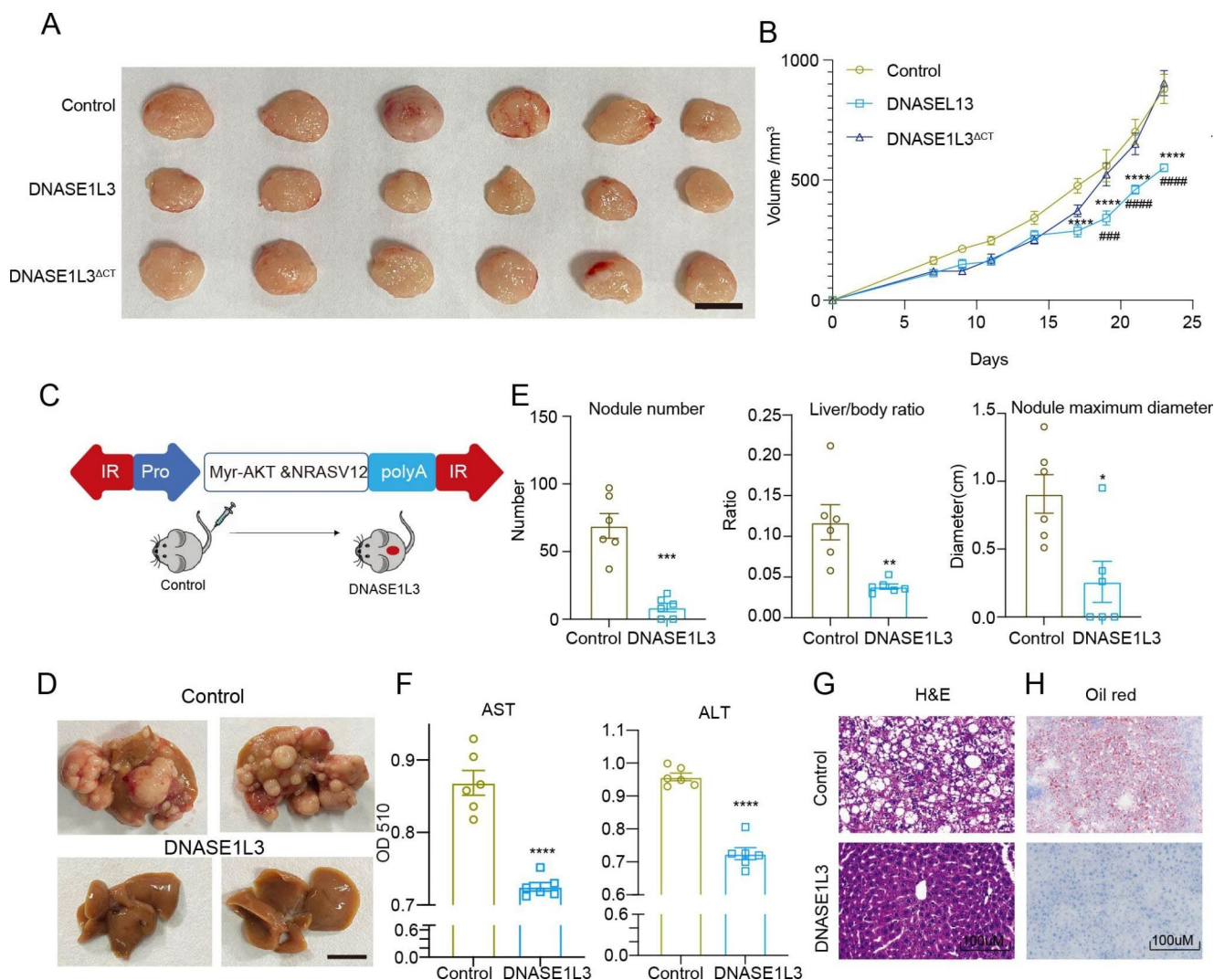


Fig. 3 DNASE1L3 inhibits HCC progress and occurrence in vivo (**A**) DNASE1L3 repressed subcutaneous tumor formation of HCCLM9 cells. Tumors were harvested from nude mice subcutaneously engrafted with Control, DNASE1L3 or DNASE1L3^{ACT} overexpression HCCLM9 cells (n=6 per group, scale bar: 1 cm). (**B**) Statistical analysis of tumor volume at different days post engraftment in nude mice as indicated. * represents significant difference between Control and DNASE1L3 group, # represents significant difference between DNASE1L3 and DNASE1L3^{ACT} group (n=6 per group). (**C**) Schematic diagram of hydrodynamic injection of transposon-based vectors expressing constitutively active AKT and NRASV12 to induce liver cancer in mice. The Control mouse group was injected with vector, AKT, NRASV12 and SB100 mixture; the experimental mouse group was injected with DNASE1L3, AKT, NRASV12 and SB100 mixture.

(**D**) Representative morphology (abdominal side, left panel; dorsal side, right panel) of livers from tumor-bearing mice (scale bar: 1 cm, 1×). Control mice exhibited worse phenotypes. (**E**) Statistical analysis showed that DNASE1L3 overexpression significantly decreased liver cancer nodule numbers, liver/body ratio, and maximal tumor diameter compared to control groups (n=6 per group) (scale bar: 1 cm, 1×). (**F**) DNASE1L3 overexpression reduced the serum level of ALT and AST (n=6 per group). (**G-H**) Histopathological analysis of liver tissues from tumor-bearing mice. Representative images of H&E staining (scale bar: 100 μm, 20×) (**G**) and Oil red staining (scale bar: 100 μm, 20×) (**H**) of tumor tissues from Control and DNASE1L3 groups were presented. Data in (**B**)(**E**)(**F**) were presented as the mean ± SEM. Data in (**B**) were analyzed by two-way ANOVA. Data in (**E**) (**F**) were analyzed by Students' t test. *p < 0.05, **p < 0.01, ***p < 0.001, ****p < 0.0001

liver cancer. Hydrodynamic injection of transposon-based vectors expressing constitutively active AKT (myr-AKT) and NRASV12 through tail vein potently caused lipid accumulation and induced mouse liver cancer (Fig. 3C) [23–25]. Apparently, DNASE1L3 overexpression significantly mitigated the development of liver cancer: A relatively normal morphology and liver texture (soft and smooth) was

observed in DNASE1L3 overexpression mice compared to a completely disrupted morphology and liver texture by various liver nodules in control mice (Fig. 3D). DNASE1L3 overexpression decreased the numbers of tumor nodules, the liver/body ratio and the maximum tumor diameter (Fig. 3E). Moreover, DNASE1L3 overexpression reduced the serum levels of ALT and AST (Fig. 3F). Histopathological analysis

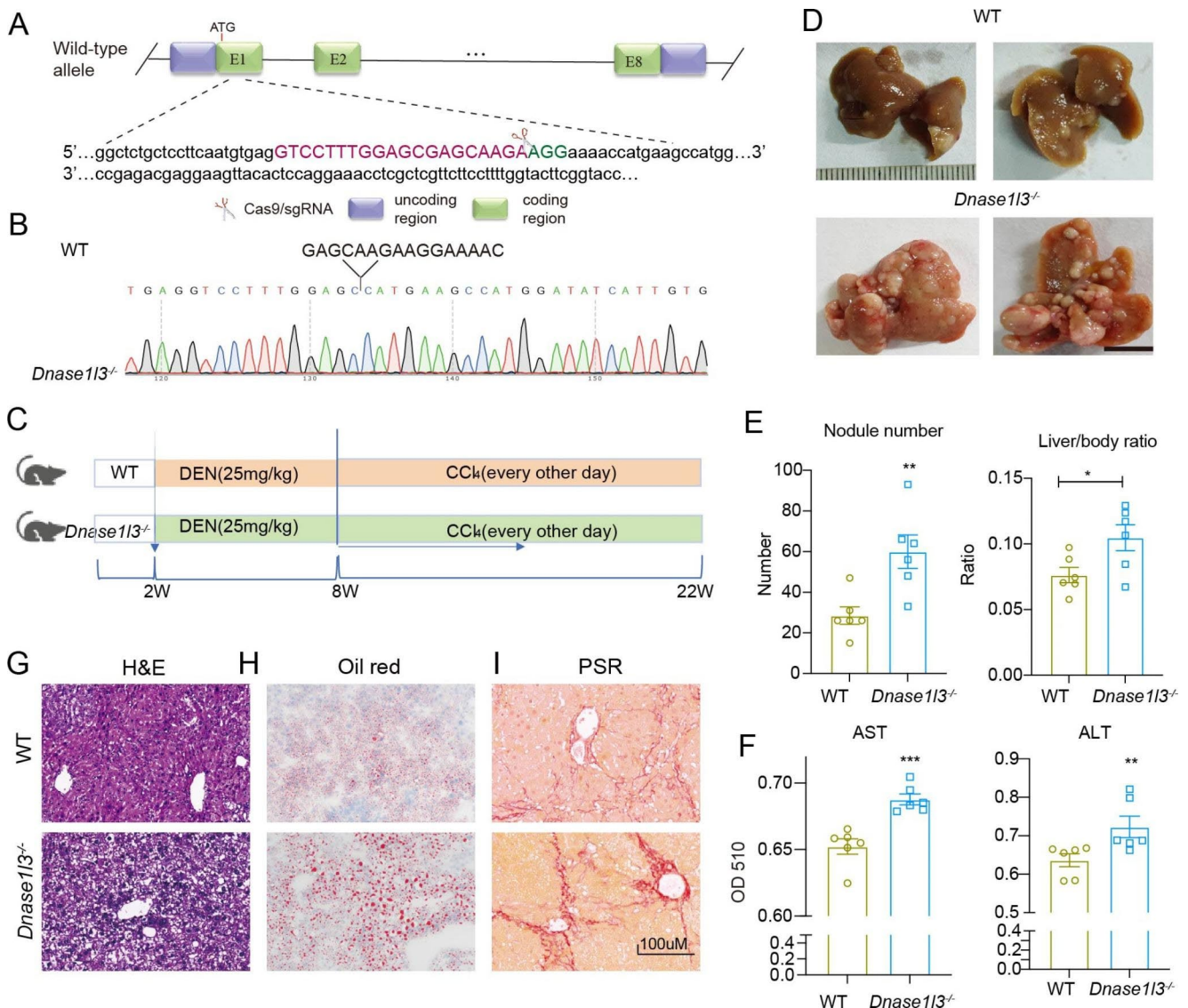


Fig. 4 DNASE1L3 deficiency promotes HCC tumorigenesis in vivo (A) Schematic diagram showed the locus and the sequence used for CRISPR/Cas9-mediated *Dnase1l3* gene knockout. (B) Genomic sequencing confirmed the deletion of 16 base pairs in exon 1 of *Dnase1l3* gene. (C) Schematic diagram of the DEN/CCl₄-induced HCC mouse model. DEN (25 mg/kg body weight) was intraperitoneally injected into 2-week-old mice and CCl₄ (40 μL 40% CCl₄) was administered through gavage every other day from week 8 to 22. (D) Representative morphology (abdominal side, left panel; dorsal side,

right panel) of livers from tumor-bearing mice (22 weeks) (scale bar: 1 cm, 1×). The *Dnase1l3*^{-/-} group showed worse phenotypes. (E-F) Statistical analysis of tumor nodule numbers, liver/body ratio (E) and serum AST/ALT (F) in WT and *Dnase1l3*^{-/-} groups (n=6 per group). (G-I) Histopathological analysis of liver tissues from tumor-bearing mice. Representative images of H&E staining (G), Oil red staining (H), and PSR staining (I) (scale bar: 100 μm, 20×) of tumor tissues from the WT and *Dnase1l3*^{-/-} groups were presented. Data in (E)(F) were presented as the mean ± SEM and analyzed by Student's t test. *p<0.05, **p<0.01, ***p<0.001, ****p<0.0001

of tumor tissues further revealed that DNASE1L3 overexpression decreased the formation of pseudo-lobules and cell vacuolation and ameliorated lipid accumulation in the liver (Fig. 3G-H). Overall, these results indicate that DNASE1L3 inhibits AKT/NRASV12-induced liver cancer in mice.

3.4 DNASE1L3 deficiency promotes HCC tumorigenesis in vivo

To further verify the in vivo function of DNASE1L3 in HCC, we generated *Dnase1l3* knockout (*Dnase1l3*^{-/-}) mice using the CRISPR/Cas9 technique (Fig. 4A). Genome sequencing confirmed a 16-nucleotide deletion in exon 1 in these mice (Fig. 4B). DEN/CCl₄ treatment induced HCC in both WT and *Dnase1l3*^{-/-} mice (Fig. 4C) [25, 26]. Noticeably,

DNASE1L3 deficiency enhanced DEN/CCl₄-induced liver cancer: *Dnase1l3*^{-/-} mice exhibited a deteriorated liver morphology and texture compared to WT mice (Fig. 4D). Livers from *Dnase1l3*^{-/-} mice showed more tumor nodules and larger sizes than those of WT mice (Fig. 4E). Moreover, serum ALT and AST levels in *Dnase1l3*^{-/-} mice were significantly increased in comparison to those in WT mice (Fig. 4F). *Dnase1l3* deficiency increased the formation of pseudo-lobules and cell vacuolation as well as blood cell infiltration (Fig. 4G), significantly augmented lipid accumulation (Fig. 4H) and worsened liver fibrosis (Fig. 4I). Together, these data indicate that *Dnase1l3* deficiency promotes DEN/CCl₄-induced HCC tumorigenesis in mice.

3.5 DNASE1L3 is a negative cell cycle regulator in HCC

To determine the mechanism underlying the suppressive role of DNASE1L3 in HCC, tumor tissues from DEN/CCl₄-treated WT and *Dnase1l3*^{-/-} mice were harvested for RNA-Seq analysis. PCA analysis revealed a distinct separation of WT and *Dnase1l3*^{-/-} groups (Fig. 5A). Volcano analysis revealed 277 differentially expressed genes (DEGs) of which 132 were downregulated and 145 were upregulated. The top 10 up-regulated (red) and down-regulated (blue) genes are highlighted (Fig. 5B). Gene Set Enrichment Analysis (GSEA)-based on KEGG pathways revealed a cell cycle signature in the top 10 upregulated pathways (Fig. 5C) and most of the enriched cell cycle genes in the *Dnase1l3*^{-/-} group were found to be upregulated (Fig. 5D). Particularly, *Cdk2*, *Ccnd1* and *Cdc25c* were consistently upregulated in DEN/CCl₄-induced *Dnase1l3*^{-/-} tumors but downregulated in AKT/NRASV12-induced DNASE1L3 overexpression tumors, whereas other genes did not show such pattern (Fig. 5E-F). Moreover, the differential expression of the Cyclin D1 and CDK2, but not CDC25C, proteins was confirmed by Western blotting (Fig. 5G-H). These observations suggest that DNASE1L3 may negatively regulate the cell cycle in HCC and that Cyclin D1 and CDK2 are potential targets for DNASE1L3.

3.6 DNASE1L3 delays cell cycle progression in HCC

To directly determine the effect of DNASE1L3 on the cell cycle in HCC, we analyzed the cell cycle profile of HCCLM9 cells overexpressing wildtype DNASE1L3 or mutant DNASE1L3^{ΔCT}. Unexpectedly, we found that neither DNASE1L3 nor mutant DNASE1L3^{ΔCT} overexpression significantly altered the cell cycle profile at basal status compared to control (Fig. 6A-B, top panels). We also tested whether DNASE1L3 affected cell cycle progression. To this end cells were arrested and synchronized at the G2/M

phase by nocodazole treatment or at the G1 phase by serum starvation (Fig. 6A-B, middle panels). We found that two hours after nocodazole withdrawal more DNASE1L3 overexpressing cells were retained at the G2/M phase and that fewer cells entered into the G1 phase than in control cells (Fig. 6A, bottom panels). Consistently, more DNASE1L3 overexpressing cells stayed at the G1 phase than control cells after serum stimulation (Fig. 6B, bottom panels). In both cases, DNASE1L3^{ΔCT} overexpressing cells behaved comparable to control cells (Fig. 6A-B). In summary, these observations suggest that DNASE1L3 overexpression delays cell cycle progression in HCCLM9 cells.

3.7 DNASE1L3 impairs cell cycle progression by interacting with CDK2

Both CDK2 and Cyclin D1 are known to play a role in G1/S progression. We found that CDK2 was downregulated at both the mRNA and protein levels in HCCLM9 cells overexpressing wildtype DNASE1L3, but not mutant DNASE1L3^{ΔCT} (Fig. 7A-B). In contrast, Cyclin D1 was not significantly downregulated at the mRNA levels (Fig. 7A-B). To test whether DNASE1L3 affects G1/S progression, we used an E2F1 reporter for dual-luciferase reporter assays. We found that DNASE1L3 overexpression effectively repressed the transcriptional activity of an E2F1-driven promoter, whereas mutant DNASE1L3^{ΔCT} had lost this ability (Fig. 7C). Moreover, CDK2 dramatically stimulated the transcriptional activity of the E2F1-driven promoter whereas DNASE1L3 partially abolished the effect (Fig. 7D). These observations suggest that DNASE1L3 affects the cell cycle by acting on CDK2. In fact, CDK2 overexpression alone led to the promotion of cell proliferation, migration and invasion (Fig. 7E-H). More importantly, CDK2 overexpression effectively antagonized the inhibitory effect of DNASE1L3 on HCCLM9 cells (Fig. 7E-H). In support of the role of DNASE1L3 on CDK2, DNASE1L3 was found to be localized in the nucleus as detected by Western blotting and immunofluorescence (Fig. 7I-J). Co-immunoprecipitation further confirmed the interaction of DNASE1L3 with CDK2 using exogenously overexpressed (Fig. 7K-L) and endogenous (Fig. 7M-N) proteins, and immunofluorescence verified the colocalization of CDK2 and DNASE1L3 in the nucleus (Fig. 7O). In addition, we found that DNASE1L3 did not interact with E2F1 (Fig. S2A). Notably, its C-terminal deletion (DNASE1L3^{ΔCT}) dramatically impaired the ability to interact with CDK2 (Fig. 7P-Q). Overall, these findings suggest that DNASE1L3 impairs HCC cell cycle progression by interacting with CDK2 and repressing CDK2-stimulated E2F1 activity.

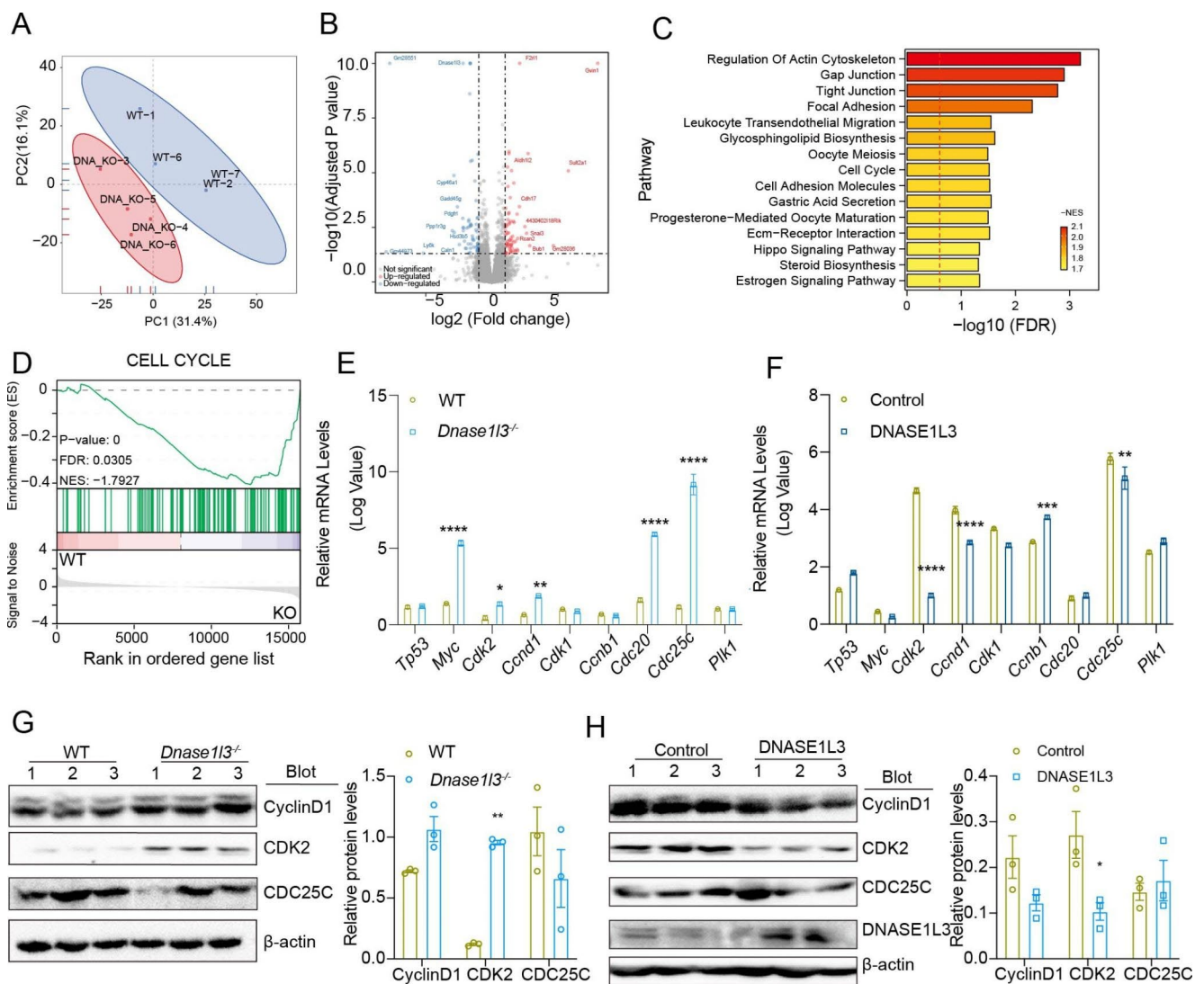


Fig. 5 DNASE1L3 is a negative regulator of cell cycle in HCC (A) PCA analysis of RNA-Seq data of DEN/CCl₄-induced HCC tumor tissues from WT and *Dnase1l3*^{-/-} mice showed distinct separation of two groups (n=4 per group). (B) Volcano analysis identified differentially expressed genes (DEGs) (upregulated genes n=145; down-regulated genes n=132). The top 10 upregulated and downregulated genes in *Dnase1l3*^{-/-} group were indicated in blue or red, respectively. (C) The top 15 KEGG pathways enriched in GSEA analysis (n=4 per group). (D) Enrichment score plot of cell cycle signature (n=4 per group). (E-F) Quantitative RT-PCR analysis confirmed the effect of

DNASE1L3 on the expression of cell cycle genes (n=3 per group). (G-H) Immunoblotting analysis (left panel) and statistical analysis of densitometry (right panel) confirmed the effect of DNASE1L3 on the expression of cell cycle genes (n=3 per group). Upregulation (E and G) was observed in HCC tumor tissues from *Dnase1l3*^{-/-} mice (DEN/CCl₄) (n=3 per group). Downregulation (F-H) was observed in HCC tumor tissues from DNASE1L3 overexpression mice (AKT/NRASV12) (n=3 per group). Data in (E)(F) and right panel in (G)(H) were presented as the mean ± SEM and analyzed by two-way ANOVA. *p<0.05, **p<0.01, ***p<0.001, ****p<0.0001

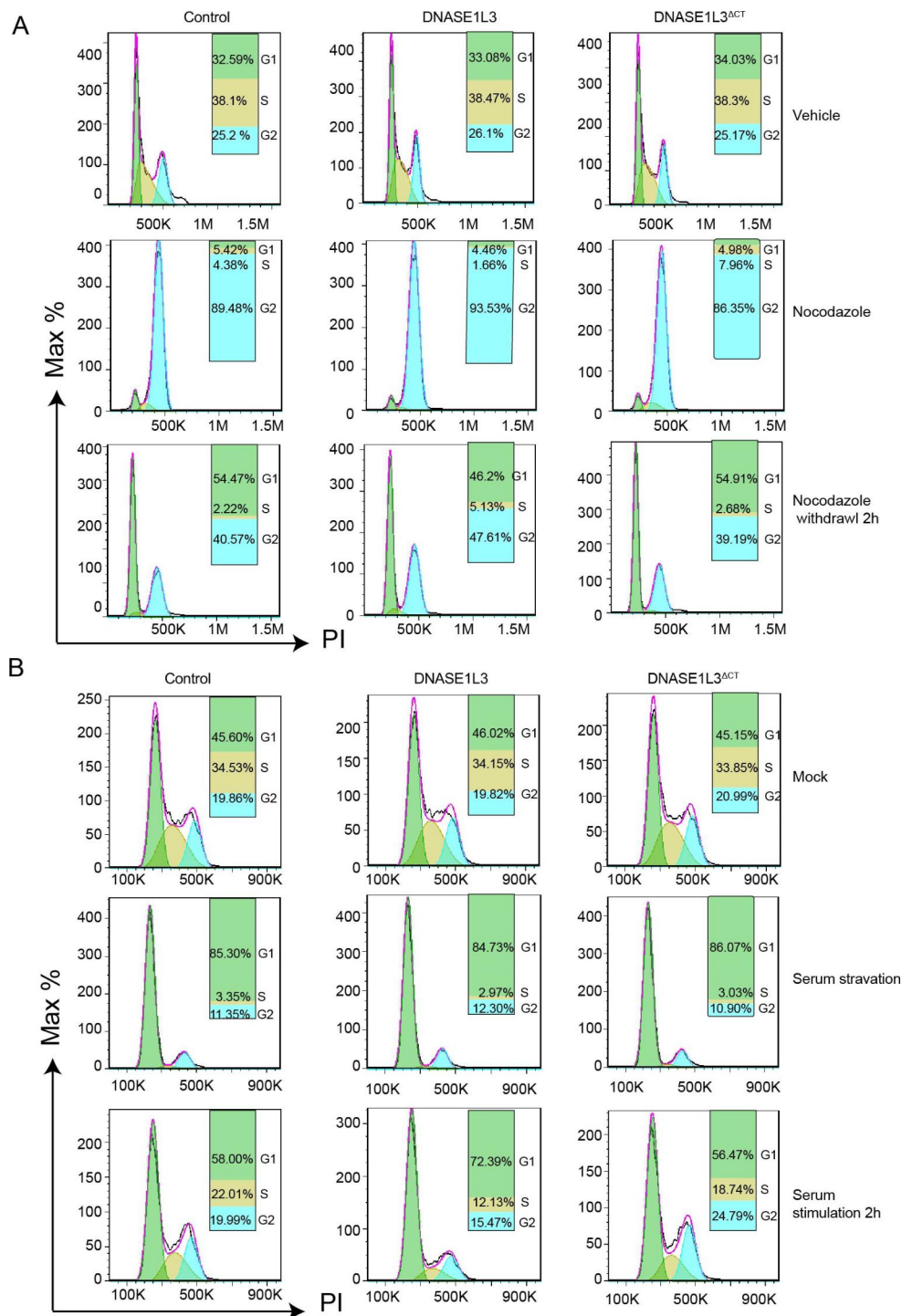
4 Discussion

As a member of the deoxyribonuclease enzyme family, DNASE1L3 is tightly associated with systemic lupus erythematosus (SLE), scleroderma/systemic sclerosis (SSc) and rheumatoid arthritis (RA) [27]. DNASE1L3 may also be a prognostic biomarker in some types of cancer [17]. However, the in vivo function of DNASE1L3 in HCC development and progression has not been fully addressed. In this study, we found that DNASE1L3 suppresses HCC by

delaying cell cycle progression, possibly through interacting with CDK2.

We found that DNASE1L3 delays cell cycle progression and suppresses HCC development. Previous studies reported an inhibitory function of DNASE1L3 in HCC cell proliferation and migration through immune escape via the CCR7/CCL19 axis [17, 20], but these conclusions were merely based on data derived from HCC cell lines and were never validated in any genetic model. Here, we found that DNASE1L3 suppresses HCC cell proliferation,

Fig. 6 DNASE1L3 delays cell cycle progress in HCC cells (**A–B**) Control, WT DNASE1L3, and DNASE1L3^{ACT} overexpression HCCLM9 cells were treated with vehicle (top panels), nocodazole (middle panels) (35 ng/ml) for 20 h, or nocodazole treatment followed by withdrawal and supplement of fresh medium for 2 h (bottom panels) (**A**). Control, WT DNASE1L3, or DNASE1L3^{ACT} overexpression HCCLM9 cells underwent mock treatment (top panels), serum starvation for 24 h (middle panels), or serum starvation followed by serum stimulation for 2 h (bottom panels). The cell cycle was measured by PI (60 μ g/ml) staining and analyzed by flow cytometry



migration and invasion in vitro. Furthermore, we verified the in vivo function in three mouse models. Specifically, two genetic models, *Dnase1l3*^{-/-} mice and transposon-mediated DNASE1L3 overexpression in mouse livers, unanimously confirmed a suppressive role of DNASE1L3 in HCC tumorigenesis. Most importantly, unbiased RNA-Seq analysis revealed a strong cell cycle signature. Cross-comparison analysis of the expression of cell cycle genes

in DEN/CCl₄-induced tumors, AKT/NRAS-induced tumors and HCCLM9 cells confirmed a consistent expression pattern of CDK2 in three groups. Biochemical assays showed that DNASE1L3 suppressed E2F1 activity and delayed cell cycle progression by interacting with CDK2. It is well-established that CDK2 activates E2F1 to promote G1/S transition through phosphorylating Rb [28, 29] and that CDK2 upregulation contributes to carcinogenesis [30–32].

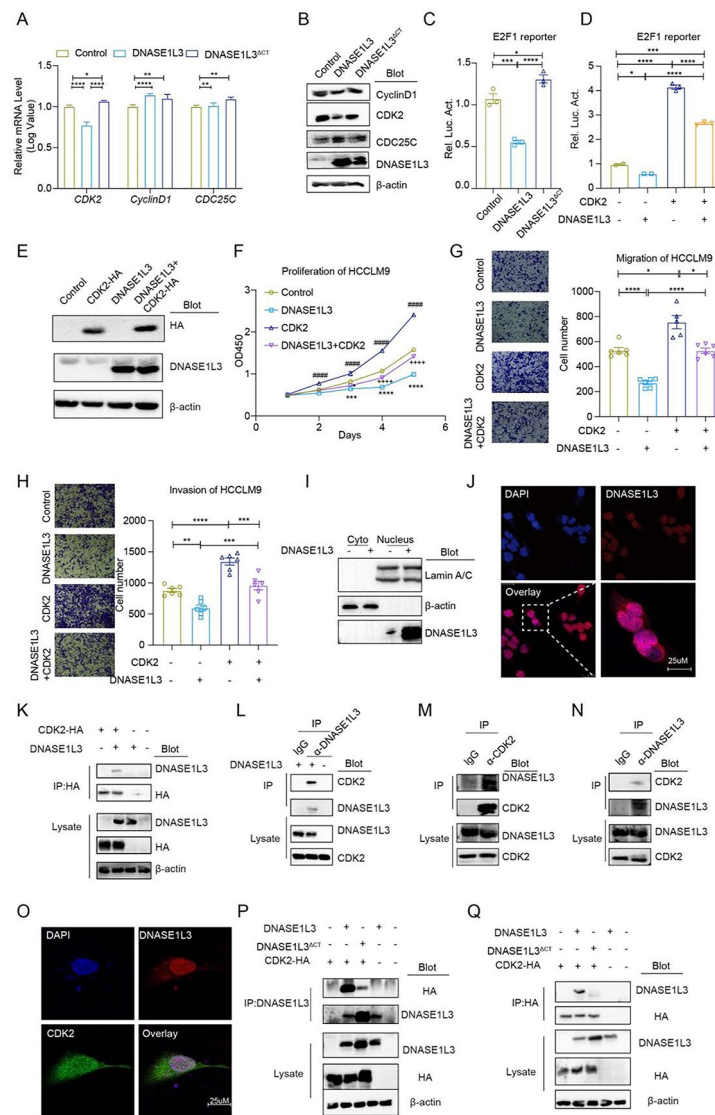


Fig. 7 DNASE1L3 functions by interacting with CDK2 (**A-B**) Quantitative RT-PCR (**A**) and immunoblotting detected the expression of cell cycle genes in Control, WT DNASE1L3, or DNASE1L3^{ACT} overexpression HCCLM9 cells. (**C**) The effect of DNASE1L3 overexpression on E2F1 activation was measured by dual-luciferase report assay using an E2F1 reporter plasmid (400 ng each) in combination with Control, DNASE1L3, or DNASE1L3^{ACT} overexpression vectors. (**D**) The effect of DNASE1L3 overexpression on CDK2-stimulated E2F1 activation was measured by dual-luciferase report assay using an E2F1 reporter plasmid (400 ng each) in combination with Control, DNASE1L3, DNSE1L3^{ACT}, or CDK2 overexpression vectors as indicated. (**E**) Immunoblotting analysis of DNASE1L3 and CDK2 overexpression in HCCLM9 cells. (**F-H**) CDK2 overexpression antagonized the inhibitory effect of DNASE1L3 on HCC cell proliferation (n=3 per group) (**F**), migration (n=6 per group) (**G**) and invasion (n=6 per group) (**H**). Cell proliferation was measured by CCK8 (* represents significant difference between Control and DNASE1L3 group, # represents significant difference between Control and CDK2 group, + represents significant difference between Control and DNASE1L3 + CDK2 group) (n=3 per group). Migration and invasion were measured by transwell (n=6 per group). The left panels were representative images and the right panels were statistical results (**G**)(**H**). (**I**) Immunoblotting showed nucleus localization of DNASE1L3 protein in Control (-) and DNASE1L3-overexpression (+) HCCLM9 cells. β-actin and Lamin A/C served as controls for proteins in cytoplasm (cyto) and

nucleus, respectively. (**J**) Representative images of immunofluorescence analysis showed nucleus localization of DNASE1L3 (scale bar: 25 μm). DNASE1L3 was stained using an antibody (red) and the nucleus was stained with DAPI (blue). (**K-L**) Coimmunoprecipitation and immunoblotting confirmed the interaction of DNASE1L3 and CDK2. HEK293T cells were transfected with DNASE1L3 (+), CDK2-HA (+) or combination (**K**). The interaction of exogenous DNASE1L3 and endogenous CDK2 in HCCLM9 cells (**L**). Coimmunoprecipitation (IP) and immunoblotting (Blot) were performed with antibodies as indicated. (**M-N**) Coimmunoprecipitation and immunoblot confirmed the interaction of the endogenous DNASE1L3 and CDK2 in HCCLM9 cells. Coimmunoprecipitation (IP) and immunoblot (Blot) were performed with antibodies as indicated. (**O**) Representative images of immunofluorescence showed colocalization of DNASE1L3 and CDK2 in nucleus in HCCLM9 cells (scale bar: 25 μm). The nucleus was stained with DAPI (blue), DNASE1L3 (red) and CDK2 (green) were stained with antibodies as indicated. (**P-Q**) C-terminal deletion impaired the interaction of DNASE1L3 and CDK2. HEK293T cells were transfected with DNASE1L3 (+) or DNASE1L3^{ACT} (+) in combination with CDK2-HA (+). Coimmunoprecipitation and immunoblotting were performed with antibodies as indicated. Data in (**A**)(**C**)(**D**) (**F**) and the right panel of (**G**)(**H**) were presented as the mean ± SEM. Data in (**A**)(**F**) was analyzed by two-way ANOVA. Data in (**C**)(**D**) and the right panel of (**G**)(**H**) were analyzed by one-way ANOVA. *p<0.05, **p<0.01, ***p<0.001, ****p<0.0001

Considering that CDK2 is also an E2F1 target gene [33], E2F1 and CDK2 may form a positive regulatory loop and promote HCC. However, the interaction between DNASE1L3 and CDK2 may suppress CDK2 activity and, subsequently, lead to a decrease of E2F1 activation, which in turn may cause downregulation of *CDK2* at the transcription level. In this way, DNASE1L3 downregulation may enhance such a positive regulatory loop and promote HCC. Therefore, manipulating the interaction between DNASE1L3 and CDK2 may serve as a new strategy to target the dysregulated cell cycle in HCC.

The conformation of DNASE1L3 appears to be essential for its inhibitory effect on HCC. In our study, we found that DNASE1L3^{ACT} lost its interaction with CDK2 and failed to suppress HCC. Accordingly, DNASE1L3^{ACT} failed to repress cell cycle progression and E2F1 activity. DNASE1L3 is a unique member of deoxyribonuclease I family, for its C-terminal domain confers DNASE1L3 with the ability to digest liposome-coated DNA and genomic DNA with native polynucleosomes. The stable-protruded α -helix in the C-terminal domain may promote the displacement of DNA from bound histones. Deletion of the C-terminal abolished the deoxyribonuclease activity of DNASE1L3 on liposome-coated DNA and genomic DNA, but not on naked DNA [14]. The defect of DNASE1L3^{ACT} may attributed to its impaired interaction with CDK2. Interestingly, a Caucasian-specific SNP R206C allele has been found to induce structural instability of the enzyme and to produce an inactive form of DNASE1L3 [14, 34]. In our study, DNASE1L3^{R206C} failed to repress cell proliferation and had lost the interaction with CDK2. Both C-terminal deletion and R206C mutation cause conformational instability. Thus, these observations suggest that integrity of the DNASE1L3 conformation is essential for its interaction with CDK2 and is required for its inhibitory function on HCC. Mutants with point mutations in active sites may help to address the question whether the endonuclease activity is really required for DNASE1L3 function.

DNASE1L3 may be involved in protecting against chronic liver injury. Multiple factors may induce chronic liver injury and, subsequently, causes liver inflammation, parenchymal injury and liver fibrosis, which increase the risk of cirrhosis and HCC [35]. In vitro, we found that DNASE1L3 did not reduce HCC cell apoptosis. However, *Dnase1l3* deficiency did increase the ALT and AST levels and worsened liver fibrosis in a DEN/CCl₄-induced mouse liver cancer model. Considering that DNASE1L3 participates in the regulation of autoimmunity such as SLE by digesting DNA [14, 36], DNASE1L3 likely digests DNA released by apoptotic HCC cells. Apoptotic HCC cells as well as DNA-containing microparticles may activate innate immune responses and inflammation, which in turn may cause the

chronic liver injury. However, the top 10 enriched signatures did not include DNA damage and immune pathways. Whether DNASE1L3 acts as a new regulator for protecting against chronic liver injury still remains to be established.

5 Conclusion

Our data indicate that DNASE1L3 is a favorable prognostic factor and is tightly associated with HCC development. We found that DNASE1L3 suppresses HCC cell proliferation, migration and invasion in vitro and dampens HCC tumorigenesis and progression in vivo. More importantly, we found that DNASE1L3 delays cell cycle progression by interacting with CDK2 and disrupting a positive E2F1-CDK2 regulatory loop in HCC cells. Our findings indicate that DNASE1L3 acts as a novel cell cycle regulator and tumor suppressor in HCC. This study may provide a basis for the development of new strategies targeting dysregulated cell cycle regulation in HCC.

Supplementary Information The online version contains supplementary material available at <https://doi.org/10.1007/s13402-022-00709-1>.

Acknowledgements We thank all the students and colleagues in our laboratory for technical support.

Authors' contributions Jiaqi Sun and Zan Huang designed the research; Jiaqi Sun, Xiyang Wang, Qingsong Shen, Min Wang performed the animal experiments; Jiaqi Sun, Qingsong Shen, Min Wang, Xuechun Zhang, Shuxian Chen performed the cell and molecular experiments. Yufeng Yuan and Zhonglin Zhang collected the patient samples. Wenhua Li provided critical reagents and technical support. Yongping Huang analyzed the RNA-seq data. Jiaqi Sun and Zan Huang wrote the paper.

Funding This research was supported by the National Natural Science Foundation of China (Grant Nos. 91957109 and 81870427 to Z. Huang).

Data Availability Full data will be available from the corresponding author upon reasonable request.

Declarations

Competing interests The authors have stated explicitly that there are no conflicts of interest in connection with this article.

Ethics approval HCC tissues and the paired adjacent non-tumor tissues were collected from Zhongnan Hospital of Wuhan University, Wuhan, China. Ethic approval was obtained from the Medical Ethics Committee of Zhongnan Hospital of Wuhan University (No.2018013). All procedures performed in this study adhere to the tenets of the *Declaration of Helsinki*.

All animal experiments were approved by the Animal Care and Use Committee of the College of Life Sciences of Wuhan University (No.16010 A), and care was provided according to the criteria outlined in the *Guide for the Care and Use of Laboratory Animals* prepared

by the National Academy of Sciences and published by the National Institutes of Health.

Consent to participate Informed consent was obtained from each patient included in this study.

Consent to publish Not applicable.

Nonstandard abbreviations AKT, serine/threonine kinase 1; CCK8, Cell Counting Kit-8; CCL₄, carbon tetrachloride; CDC20, cell division cycle 20; CDC25C, cell division cycle 25 C; CDK, cyclin dependent kinase; CDK2, cyclin dependent kinase 2; DNA, deoxyribonucleic acid; DNASE1L3, deoxyribonuclease I like 3; DEN, diethylnitrosamine; E2F1, E2F transcription factor 1; gRNA, guide RNA; GSEA, Gene Set Enrichment Analysis; HCC, hepatocellular carcinoma; HE, hematoxylin-eosin; KEGG, Kyoto Encyclopedia of Genes and Genomes; NET, Neuroendocrine tumor; NRASV12, NRAS proto-oncogene G12V; PCA, Principal Component Analysis; PSR, Picric Sirius red; RNA-Seq, RNA sequencing; RTCA, Real Time Cell Analysis; WT, wild type.

References

- Z. Chen, H. Xie, M. Hu, T. Huang, Y. Hu, N. Sang, Y. Zhao, Recent progress in treatment of hepatocellular carcinoma. *Am. J. Cancer Res.* **10**, 2993–3036 (2020)
- T. Otto, P. Sicinski, Cell cycle proteins as promising targets in cancer therapy. *Nat. Rev. Cancer* **17**, 93–115 (2017)
- A. Jindal, A. Thadi, K. Shailubhai, Hepatocellular Carcinoma: Etiology and Current and Future Drugs. *J. Clin. Exp. Hepatol.* **9**, 221–232 (2019)
- X. Qing, W. Xu, J. Zong, X. Du, H. Peng, Y. Zhang, Emerging treatment modalities for systemic therapy in hepatocellular carcinoma. *Biomark. Res* **9**, 64 (2021)
- M. Malumbres, M. Barbacid, Cell cycle, CDKs and cancer: a changing paradigm. *Nat. Rev. Cancer* **9**, 153–166 (2009)
- R. Beroukhi, C.H. Mermel, D. Porter, G. Wei, S. Raychaudhuri, J. Donovan, J. Barretina, J.S. Boehm, J. Dobson, M. Urashima, K.T. Mc Henry, R.M. Pinchback, A.H. Ligon, Y.-J. Cho, L. Haery, H. Greulich, M. Reich, W. Winckler, M.S. Lawrence, B.A. Weir, K.E. Tanaka, D.Y. Chiang, A.J. Bass, A. Loo, C. Hoffman, J. Prensner, T. Liefeld, Q. Gao, D. Yecies, S. Signoretti, E. Maher, F.J. Kaye, H. Sasaki, J.E. Tepper, J.A. Fletcher, J. Taberero, J. Baselga, M.-S. Tsao, F. Demichelis, M.A. Rubin, P.A. Janne, M.J. Daly, C. Nucera, R.L. Levine, B.L. Ebert, S. Gabriel, A.K. Rustgi, C.R. Antonescu, M. Ladanyi, A. Letai, L.A. Garraway, M. Loda, D.G. Beer, L.D. True, A. Okamoto, S.L. Pomeroy, S. Singer, T.R. Golub, E.S. Lander, G. Getz, Sellers, W. R., and Meyerson, M. The landscape of somatic copy-number alteration across human cancers. *Nature* **463**, 899–905 (2010)
- S. Akli, C.S. Van Pelt, T. Bui, L. Meijer, K. Keyomarsi, Cdk2 is required for breast cancer mediated by the low-molecular-weight isoform of Cyclin E. *Cancer Res.* **71**, 3377–3386 (2011)
- Y. Hoshida, S.M. Nijman, M. Kobayashi, J.A. Chan, J.P. Brunet, D.Y. Chiang, A. Villanueva, P. Newell, K. Ikeda, M. Hashimoto, G. Watanabe, S. Gabriel, S.L. Friedman, H. Kumada, J.M. Llovet, T.R. Golub, Integrative transcriptome analysis reveals common molecular subclasses of human hepatocellular carcinoma. *Cancer Res.* **69**, 7385–7392 (2009)
- S. Rebouissou, J.C. Nault, Advances in molecular classification and precision oncology in hepatocellular carcinoma. *J. Hepatol.* **72**, 215–229 (2020)
- K. Schulze, J.C. Nault, A. Villanueva, Genetic profiling of hepatocellular carcinoma using next-generation sequencing. *J. Hepatol.* **65**, 1031–1042 (2016)
- W.F. Baron, C.Q. Pan, S.A. Spencer, A.M. Ryan, R.A. Lazarus, K.P. Baker, Cloning and characterization of an actin-resistant DNase I-like endonuclease secreted by macrophages. *Gene* **215**, 291–301 (1998)
- M. Napirei, S. Ludwig, J. Mezrhah, T. Klöckl, H.G. Mannherz, Murine serum nucleases - contrasting effects of plasmin and heparin on the activities of DNase I and DNase I-like 3 (DNase I13). *FEBS J.* **276**, 1059–1073 (2009)
- A. Wilber, M. Lu, M.C. Schneider, Deoxyribonuclease I-like III is an inducible macrophage barrier to liposomal transfection. *Mol. Ther.* **6**, 35–42 (2002)
- V. Sisirak, B. Sally, V. D'Agati, W. Martinez-Ortiz, Z.B. Ozcarar, J. David, A. Rashidfarrokhi, A. Yeste, C. Panea, A.S. Chida, M. Bogunovic, I.I. Ivanov, F.J. Quintana, I. Sanz, K.B. Elkon, M. Tekin, F. Yalcinkaya, T.J. Cardozo, R.M. Clancy, J.P. Buyon, B. Reizis, Digestion of chromatin in apoptotic cell microparticles prevents autoimmunity. *Cell* **166**, 88–101 (2016)
- P.S. Tsou, A.H. Sawalha, Unfolding the pathogenesis of scleroderma through genomics and epigenomics. *J. Autoimmun.* **83**, 73–94 (2017)
- M. Jiménez-Alcázar, C. Rangaswamy, R. Panda, J. Bitterling, Y.J. Simsek, A.T. Long, R. Bilyy, V. Krenn, C. Renné, T. Renné, S. Kluge, U. Panzer, R. Mizuta, H.G. Mannherz, D. Kitamura, M. Herrmann, M. Napirei, T.A. Fuchs, Host DNases prevent vascular occlusion by neutrophil extracellular traps. *Science* **358**, 1202–1206 (2017)
- Z. Deng, M. Xiao, D. Du, N. Luo, D. Liu, T. Liu, D. Lian, J. Peng, DNASE1L3 as a prognostic biomarker associated with immune cell infiltration in cancer. *Onco Targets Ther* **14**, 2003–2017 (2021)
- J. Liu, J. Yi, Z. Zhang, D. Cao, L. Li, Y. Yao, Deoxyribonuclease I-like 3 may be a potential prognostic biomarker associated with immune infiltration in colon cancer. *Aging (Albany NY)* **13**, 16513–16526 (2021)
- S. Wang, H. Ma, X. Li, X. Mo, H. Zhang, L. Yang, Y. Deng, Y. Yan, G. Yang, X. Liu, H. Sun, DNASE1L3 as an indicator of favorable survival in hepatocellular carcinoma patients following resection. *Aging (Albany NY)* **12**, 1171–1185 (2020)
- D. Guo, D. Ma, P. Liu, J. Lan, Z. Liu, Q. Liu, DNASE1L3 arrests tumor angiogenesis by impairing the senescence-associated secretory phenotype in response to stress. *Aging (Albany NY)* **13**, 9874–9899 (2021)
- M. Wang, T. Zhang, X. Zhang, Z. Jiang, M. Peng, Z. Huang, BMP2K dysregulation promotes abnormal megakaryopoiesis in acute megakaryoblastic leukemia. *Cell. Biosci.* **10**, 57 (2020)
- Z. Huang, T.D. Richmond, A.G. Muntean, D.L. Barber, M.J. Weiss, J.D. Crispino, STAT1 promotes megakaryopoiesis downstream of GATA-1 in mice. *J. Clin. Invest.* **117**, 3890–3899 (2007)
- C. Ho, C. Wang, S. Mattu, G. Destefanis, S. Ladu, S. Delogu, J. Armbruster, L. Fan, S.A. Lee, L. Jiang, F. Dombrowski, M. Evert, X. Chen, D.F. Calvisi, AKT (v-akt murine thymoma viral oncogene homolog 1) and N-Ras (neuroblastoma ras viral oncogene homolog) coactivation in the mouse liver promotes rapid carcinogenesis by way of mTOR (mammalian target of rapamycin complex 1), FOXM1 (forkhead box M1)/SKP2. *Hepatology* **55**, 833–845 (2012)
- J.K. Stauffer, A.J. Scarzello, J.B. Andersen, R.L. De Kluyver, T.C. Back, J.M. Weiss, S.S. Thorgeirsson, R.H. Wiltrout, Coactivation of AKT and β -Catenin in mice rapidly induces formation of lipogenic liver tumors. *Cancer Res.* **71**, 2718–2727 (2011)
- B.A. Diwan, J.M. Rice, J.M. Ward, Strain-dependent effects of phenobarbital on liver tumor promotion in inbred mice. *Prog. Clin. Biol. Res.* **331**, 69–83 (1990)

26. T. Uehara, G.R. Ainslie, K. Kutanzi, I.P. Pogribny, L. Muskhe-lishvili, T. Izawa, J. Yamate, O. Kosyk, S. Shymonyak, B.U. Bradford, G.A. Boorman, R. Bataller, I. Rusyn, Molecular mech-anisms of fibrosis-associated promotion of liver carcinogenesis. *Toxicol. Sci.* **132**, 53–63 (2013)
27. L.N. Coke, H. Wen, M. Comeau, M.H. Ghanem, A. Shih, C.N. Metz, W. Li, C.D. Langefeld, P.K. Gregersen, K.R. Simpfendorfer, Arg206Cys substitution in DNASE1L3 causes a defect in DNASE1L3 protein secretion that confers risk of systemic lupus erythematosus. *Ann. Rheum. Dis.* **80**, 782–787 (2021)
28. M. Malumbres, M. Barbacid, To cycle or not to cycle: a critical decision in cancer. *Nat. Rev. Cancer* **1**, 222–231 (2001)
29. S.A. Ezhevsky, A. Ho, M. Becker-Hapak, P.K. Davis, S.F. Dowdy, Differential regulation of retinoblastoma tumor suppressor pro-tein by g1 cyclin-dependent kinase complexes in vivo. *Mol. Cell. Biol.* **21**, 4773–4784 (2001)
30. S. Campaner, M. Doni, P. Hydbring, A. Verrecchia, L. Bianchi, D. Sardella, T. Schleker, D. Perna, S. Tronnersjo, M. Murga, O. Fernandez-Capetillo, M. Barbacid, L.G. Larsson, B. Amati, Cdk2 suppresses cellular senescence induced by the c-myc oncogene. *Nat. Cell. Biol.* **12**, 54–59 (2010)
31. J. Du, H.R. Widlund, M.A. Horstmann, S. Ramaswamy, K. Ross, W.E. Huber, E.K. Nishimura, T.R. Golub, D.E. Fisher, Critical role of CDK2 for melanoma growth linked to its melanocyte-spe-cific transcriptional regulation by MITF. *Cancer Cell.* **6**, 565–576 (2004)
32. D. Ray, Y. Terao, K. Christov, P. Kaldis, H. Kiyokawa, Cdk2-null mice are resistant to ErbB-2-induced mammary tumorigenesis. *Neoplasia* **13**, 439–444 (2011)
33. A.S. Tin, S.N. Sundar, K.Q. Tran, A.H. Park, K.M. Poindexter, G.L. Firestone, Antiproliferative effects of artemisinin on human breast cancer cells requires the downregulated expression of the E2F1 transcription factor and loss of E2F1-target cell cycle genes. *Anticancer Drugs* **23**, 370–379 (2012)
34. M. Ueki, H. Takeshita, J. Fujihara, R. Iida, I. Yuasa, H. Kato, A. Panduro, T. Nakajima, Y. Kominato, T. Yasuda, Caucasian-spe-cific allele in non-synonymous single nucleotide polymorphisms of the gene encoding deoxyribonuclease I-like 3, potentially rel-evant to autoimmunity, produces an inactive enzyme. *Clin. Chim. Acta* **407**, 20–24 (2009)
35. S. Lotersztajn, B. Julien, F. Teixeira-Clerc, P. Grenard, A. Mallat, HEPATIC FIBROSIS: Molecular Mechanisms and Drug Targets. *Annu. Rev. Pharmacol. Toxicol.* **45**, 605–628 (2005)
36. S.M. Al-Mayouf, A. Sunker, R. Abdwani, S.A. Arawi, F. Almur-shedi, N. Alhashmi, A. Sonbul, A. Sewairi, W. Qari, A. Abdal-lah, E. Al-Owain, M. Al Motywee, S. Al-Rayes, H. Hashem, M. Khalak, H. Al-Jebali, L., and F.S. Alkuraya, Loss-of-function variant in DNASE1L3 causes a familial form of systemic lupus erythematosus. *Nat. Genet.* **43**, 1186–1188 (2011)

Publisher's Note Springer Nature remains neutral with regard to juris-dictional claims in published maps and institutional affiliations.

Springer Nature or its licensor holds exclusive rights to this article under a publishing agreement with the author(s) or other rightsholder(s); author self-archiving of the accepted manuscript version of this arti-cle is solely governed by the terms of such publishing agreement and applicable law.